

Markov Random Field Modeling for Three-dimensional Reconstruction of the Left Ventricle in Cardiac Angiography

Rubén Medina, *Member, IEEE*, Mireille Garreau*, Javier Toro, Hervé Le Breton, Jean-Louis Coatrieux,
Fellow, IEEE, and Diego Jugo

Abstract

This paper reports on a method for left ventricle three-dimensional reconstruction from two orthogonal ventriculograms. The proposed algorithm is voxel-based and takes into account the conical projection geometry associated with the biplane image acquisition equipment. The reconstruction process starts with an initial ellipsoidal approximation derived from the input ventriculograms. This model is subsequently deformed in such a way as to match the input projections. To this end, the object is modeled as a three-dimensional Markov-Gibbs random field, and an energy function is defined so that it includes one term that models the projections compatibility and another one that includes the space-time regularity constraints. The performance of this reconstruction method is evaluated by considering the reconstruction of mathematically synthesized phantoms and two 3-D binary databases from two orthogonal synthesized projections. The method is also tested using real biplane ventriculograms. In this case, the performance of the reconstruction is expressed in terms of the projection error, which attains values between 9.50% and 11.78% for two biplane sequences including a total of 55 images.

Index Terms

Three-dimensional reconstruction, Markov Random Fields, Ventriculographic images, Reconstruction from projections, Simulated annealing

I. INTRODUCTION

The three-dimensional reconstruction of the ventricular shape is useful for diagnosis and for guiding interventional procedures. Information about the patient-specific three-dimensional ventricular shape improves the precision of

Manuscript received September 06, 2005.

R. Medina, J. Toro and D. Jugo are with Grupo de Ingeniería Biomédica (GIBULA), Universidad de Los Andes, Mérida, Venezuela.

M. Garreau and J. L. Coatrieux are with Laboratoire de Traitement du Signal et de L'Image (LTSI), INSERM, Université de Rennes 1, France.

H. L. Breton is with Laboratoire de Traitement du Signal et de L'Image (LTSI), INSERM, Université de Rennes 1, France and with Service d'Hémodynamique et de Cardiologie Interventionnelle, CHU Rennes, France.

* Corresponding author, Email: mireille-garreau@univ-rennes1.fr

assessment of the ventricular function, the extraction of the 3-D ventricle motion during the cardiac cycle, as well as the visualization of the observed structure from any arbitrary orientation or slicing.

Even when several imaging modalities are used in cardiological studies, up to now, X-ray angiography has been the gold standard in clinical cardiac work. This imaging modality enables real time cardiac imaging as required in interventional procedures where single plane or biplane image sequences are acquired. The acquisition is performed after guiding a catheter into the chambers of the heart or vessels and injecting a contrast agent.

Three-dimensional object reconstruction from two-dimensional projections can be considered as a particular case of the classical reconstruction problem found in tomography [1]. However, this problem is ill-posed and a robust solution is only reached by considering prior knowledge, appropriate shape primitives and assumptions. The 3-D reconstruction problem from two projections has been tackled by several research groups by assuming a homogeneous mixture of blood and contrast agent in the cavity, and by decomposing the problem into several 2-D slice reconstruction sub-problems [2]–[8]. The 3-D reconstructed object is then assembled by stacking the 2-D reconstructed binary slices. These approaches work under the assumption of a parallel projection geometry. The slice-based reconstruction approach has the disadvantage of requiring additional pre-processing stages such as projection alignment between both views. The accuracy of the results is affected by the magnification associated with the actual conical projection geometry. The method proposed by Prause and Onnash [9] considers the real oblique projection geometry but performs the reconstruction on a slice basis. Recently, Moriyama *et al.* [10] and Sato *et al.* [11] proposed an approach that recovers the left ventricle shape from multi-view X-ray cineangiograms. This approach is based on the recovery of shape from occluding contours. However, the gray-level values of acquired ventriculograms, which provide valuable information on depth, are not exploited in the reconstruction process. Kehl *et al.* [12] have also proposed a method that performs the 3-D reconstruction of cardiac chambers from multi-view rotational biplane angiographic sequences. The reconstruction is based on a tomography analytical cone-beam back-projection approach from views acquired at the same cardiac phase. The approach is voxel-driven and has the advantage of performing the 3-D reconstruction without requiring prior segmentation of the cardiac structures. Yet, it requires a large number of views to accomplish the computerized tomographic reconstruction. As a consequence, it can be affected by patient motion and contrast dye dilution.

This work is part of a project [13], [14], where a slice based reconstruction method [15], a fuzzy and evidential approach [16] as well as an evolutionary reconstruction method [17] have been explored. In [14], the first developments of the Markov Random Field based reconstruction approach are presented. However, only a 3-D Markov model is used and results are limited to the reconstruction of a binary database and a single pair of angiograms. In [16] a method for performing the binary reconstruction from two views is reported. The method is based on the fuzzy set theory and the Dempster–Shafer combination rules in order to cope with the imprecision and ambiguity of the reconstruction process. In this paper, we propose a voxel-based left ventricle 3-D reconstruction approach from two projections that considers the real conical acquisition geometry (see Fig. 1). The proposed reconstruction algorithm starts with an ellipsoidal approximation of the left ventricle shape which is subsequently deformed to reach a final 3-D shape. The algorithm uses a Markov Random Field (MRF) framework for defining a cost function

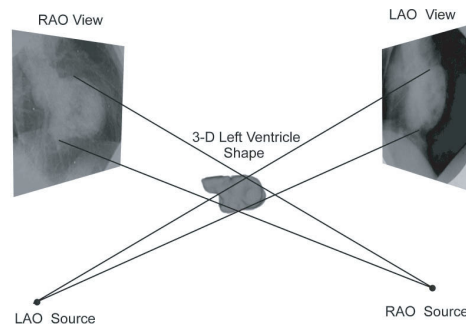


Fig. 1. Three-dimensional reconstruction of the left ventricle from two views.

involving the difference between the input images (the conventional Left Anterior Oblique (LAO) 60° and Right Anterior Oblique (RAO) 30° views) and computed projections as well as the space-time connectivity of the ventricular cavity. This energy function is then minimized by using a stochastic optimization procedure based on the Metropolis algorithm and simulated annealing [18].

The MRF theory provides a convenient and consistent way for modeling content dependent entities such as image pixels or voxels and correlated features [19]–[21]. This theory has been used for modeling and solving several problems in image processing such as image segmentation [18], texture modeling and classification [22], 3-D reconstruction of coronary sections [23], surface reconstruction [20] and motion estimation and segmentation [24]. More precisely, the MRF model takes into account non-linear interactions between the site labels and the observation process to represent an energy function term.

II. METHODS

The proposed left ventricle reconstruction method is composed of two stages. First, an approximate ellipsoidal shape is obtained by considering several geometrical features of the input images. Next, this approximation is progressively improved by considering the constraints involved in the reconstruction problem. These constraints are coded in an energy function associated with a Gibbs probability distribution of a MRF. The minimization of this energy function guides the reconstruction procedure.

A. Preprocessing Input Images

The angiograms are corrected for geometric distortion using the following procedure: a) the images of a 2-D grid are acquired using the gantry settings that will be used for the patient image acquisition; b) a dewarping polynomial is estimated using the actual and measured coordinates of the grid interception points, and c) the angiograms are corrected using the dewarping polynomial. Logarithmic subtraction is performed on ventriculograms acquired before and after the injection of a contrast agent. This is aimed at obtaining an image whose intensity value, at each pixel location, is proportional to depth in the left ventricle. In the proposed method, it is assumed that subtracted ventriculograms display only information about the left ventricle. This can be ensured by segmenting out any other

structure that may be present in the acquired images. Input images are represented by $N_4 \times N_5$ arrays, denoted as \mathbf{d}_1 and \mathbf{d}_2 respectively. The conical projection is considered in order to model the ventriculograms acquisition geometry (pinhole model). Such a model is represented by a 3×4 projection matrix denoted as \mathbf{M} . The projection is modeled as the composition of two transformations: the first one is related to the perspective projection and performs the transformation between a 3-D point expressed in the camera coordinate system and a 2-D point expressed in the image coordinate system. The second one performs the transformation between a 3-D point expressed in the object coordinate system and the camera coordinate system. The composition of both transformations is represented by matrix \mathbf{M} . The relation in homogeneous coordinates between an image point (u, v) and an object point (x, y, z) is expressed as:

$$\lambda \cdot [u \ v \ 1]^T = \mathbf{M} \cdot [x \ y \ z \ 1]^T \quad (1)$$

where λ is any non-zero scalar. As we are dealing with two views acquired with a biplane system, each source-detector of this system is modeled by a projection matrix, denoted as \mathbf{M}_1 and \mathbf{M}_2 . The elements of these matrices are estimated according to a calibration procedure [25] that involves imaging a plexiglass cube that includes a set of L lead markers. The 3-D locations $P_i(x, y, z)$ ($i = 1, \dots, L$) of the lead markers are known as well as their corresponding 2-D projections $p_i(u, v)$. An equation system of $2L$ equations with 11 unknowns corresponding to the elements of matrix \mathbf{M} is obtained by explicit evaluation of (1) (one of the elements of this matrix is $m_{34} = 1$). This system of equations can be solved when at least 6 markers are located in the cube. In this way, the relation between actual 3-D locations and pixels in the projected image is established.

B. Images Synthesis

During the reconstruction procedure it is necessary to establish a comparison between the ventriculograms and the projections of the object in reconstruction denoted as \mathbf{h}_1 and \mathbf{h}_2 , each one represented by an $N_4 \times N_5$ array. These projections are synthesized by using the pinhole model and an adaptation of a ray-tracing algorithm [26]. In this case, for each ray cast the intensity assigned in the image is the length of the interception between the ray and the binary object [27].

C. Approximate Reconstruction

The objective of the first stage is to obtain an approximate reconstructed shape. This 3-D object is an ellipsoid whose size and placement are derived from the input projections. The following assumptions are made:

- 1) The parameters defining the projection geometry are given.
- 2) The LV has been segmented on both input images.
- 3) The conical projection of the inertial center of the 3-D object matches at least approximately the inertial center estimated from the 2-D projections.

The last assumption is based on the invariance property of geometric moments in relation to translation, rotation and scale modification, which are building blocks of the projective geometry [28]. The approximate reconstruction

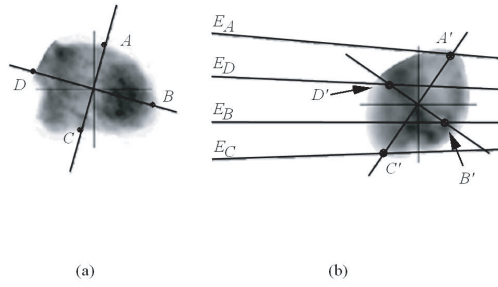


Fig. 2. The inertial axes overlaid to the segmented images. (a) RAO Projection. (b) LAO Projection.

is obtained by determining in both projections a set of points associated with the size and orientation of the 2-D shape. Using an approximate matching between points in both projections, the 3-D reconstruction is performed. The centered moment matrix for the reconstructed 3-D points is obtained and an ellipsoid is derived from this information [29].

1) *The inertial moments*: The geometrical moment is a mathematical tool that enables the recovery of features associated with size, position and orientation of the LV in the 3-D space and in the projection spaces [30]. Any object can be approximated by its mass, the gravity center position and the inertia matrix expressed in relation to the gravity center. Considering a projection image \mathbf{d} , the elements of the moment matrix are given according to:

$$m_{pq} = \sum_{i=1}^{N_4} \sum_{j=1}^{N_5} i^p j^q d_{ij} \quad (2)$$

where p, q represent the order of the inertial moment and d_{ij} is the intensity of each pixel in the image. The estimation of the coordinates of the gravity center i_{gc} and j_{gc} on each projection are given by:

$$i_{gc} = \frac{m_{10}}{m_{00}}, \quad j_{gc} = \frac{m_{01}}{m_{00}}. \quad (3)$$

This point is the origin of a coordinate system that allows the description of the object represented in the image. The moment matrix elements, estimated by taking as the reference the coordinate system positioned at the gravity center, can be obtained by using the following expression:

$$m_{gh} = \sum_{i=1}^{N_4} \sum_{j=1}^{N_5} (i - i_{gc})^g (j - j_{gc})^h d_{ij}, \quad (4)$$

where g, h represent the order of the inertial moment. By evaluating (4) considering $g, h \in \{0, 1\}$, a 2×2 moments matrix denoted as H can be obtained whose eigenvectors define the object orientation in the image. Matrix H is evaluated from the segmented and smoothed version of the input images in order to reduce the inaccuracy related to intensity variations inside the object. In Fig. 2 the inertia axes are shown overlapped on the ventriculographic RAO image and denoted as the line segments (AC) and (BD) (see Fig. 2a). The inertia axes overlapped on the ventriculographic LAO projection are denoted as (A'C') and (B'D') (see Fig. 2b). The intersection of the inertia axes (AC and BD) with the detected contour in the RAO projection defines a set of four points denoted as $\{A, B, C, D\}$.

The epipolar lines for these points are traced in the LAO view given the line segments $\{E_A, E_B, E_C, E_D\}$. The interceptions of the epipolar lines with the inertia axes in the LAO projection give the points $\{A', B', C', D'\}$. As only a rough approximation is required, the points in the RAO image are considered matched to the points in the LAO image forming the following pairs (A, A') , (B, B') , (C, C') and (D, D') (using the epipolar geometry [31]). In fact (A, A') and (C, C') are really approximate corresponding pairs whereas (D, D') and (B, B') might not be in real correspondence. As the intersection between the epipolar lines E_D and E_B are two line segments respectively, then any point in the first line segment can be in correspondence with point D and also any point in the second line segment can be in correspondence with point B. So from the epipolar constraint alone, clearly, any chosen correspondence is only a guess. However, as only a rough approximated shape is researched in this first step of the reconstruction process, the only constraints used are given by the epipolar lines on which both points D' and B' have been chosen. Results on synthesized objects and binary databases show that the second stage is able to cope with the imprecision related to the initial approximate shape. For these matched points the 3-D reconstruction is performed to obtain four 3-D points. Additionally, the gravity center in both images are considered matched and reconstructed in 3-D, thus providing the gravity center for the 3-D object. As both projections are logarithmically subtracted in order to attenuate non-contrasted structures, the projection of the gravity center in each image corresponds to a pixel whose gray-level value can be taken as an approximate to the depth of the contrasted 3-D left ventricle cavity along the projection line [9]. As the target shape is an ellipsoid that is symmetrical with respect to the gravity center, the depth (pixel value) is distributed symmetrically with respect to the gravity center along the projection line. This procedure is performed for each projection image to obtain a set of four additional 3-D points.

2) *Ellipsoid construction*: A representation of an ellipsoid as a 3×3 symmetric positive-semidefinite matrix X is considered [29], [32]. A three-dimensional volume enclosed by an ellipsoid centered at the origin is represented by a set of points z given by:

$$\{z \mid z^T X^{-1} z \leq 1, z \in \mathbb{R}^3\}. \quad (5)$$

The objective is to obtain an ellipsoidal volume shape centered at the gravity center based on the set of points previously obtained. With this purpose, the 3-D moment matrix for the set of nine points is calculated. This matrix satisfies the requirements for representing an ellipsoid whose size and orientation can be recovered through an eigen decomposition procedure [33]. Specifically, if λ_i, ν_i are the eigenvalues and eigenvectors of the matrix X , then the principal axes of the ellipsoid are in the direction given by ν_i and the corresponding semi-axes lengths are given by $\sqrt{\lambda_i}$. The ellipsoidal volume shape is obtained using (5).

D. Reconstruction based on a Markov Random Field

The approximate reconstruction provided by the previously described procedure is deformed by means of an iterative algorithm that is based on the binary MRF modeling. This procedure includes several stages that are described below.

1) *Three-dimensional binary object Markov Model*: The MRF model for the binary object in reconstruction (the Left Ventricle (LV)) takes into account the relation between the global and local 3-D LV contour probabilistic properties. The binary MRF is defined on the contour of the LV. An iterative deformation procedure based on this model is then used to improve the reconstructed shape. The gray-level value associated with each pixel in the input images is related to the depth length of the three-dimensional left ventricle according to the path of an X-ray for this projection point. This relation is used to recover the three-dimensional binary shape of the ventricle from the input images. The three-dimensional binary object in reconstruction is denoted by a realization $\mathbf{f} = \{f_{ijk}\}$ of a 3-D Random Field $\mathbf{F} = \{F_{ijk}\}$, associated with the space Ω defined in N^3 spanning all possible realizations. The sites in the Random Field are defined by the following set representing a 3-D lattice:

$$\mathbf{L} = \{(i, j, k) : 1 \leq i \leq N_1, 1 \leq j \leq N_2, 1 \leq k \leq N_3\}. \quad (6)$$

This lattice comprises $(N_1 \times N_2 \times N_3)$ voxels or sites. The 3-D object is modeled by a random field $\{F_{ijk}\}$, where each label takes on the value 1 if the voxel belongs to the ventricle and zero otherwise ($f_{ijk} \in \Lambda = \{0, 1\}$). \mathbf{F} is considered as a MRF in relation to a neighborhood:

$$\eta_{ijk} = \{(q, r, s) \in \mathbf{L} : \text{dist}((q, r, s), (i, j, k)) \leq u, (q, r, s) \neq (i, j, k)\} \quad (7)$$

where $\text{dist}(\cdot)$ denotes the Euclidean distance and u is an integer value. The MRF conditional probability is given by:

$$P(f_{ijk} | f_{\mathbf{L} - (i,j,k)}) = P(f_{ijk} | f_{\eta_{ijk}}). \quad (8)$$

According to the Hammersley-Clifford theorem [20], the random Field \mathbf{F} defined in \mathbf{L} is a Gibbs Random Field in relation to a neighborhood η if and only if the probability distribution function is given by:

$$P(\mathbf{f}) = \frac{e^{-U_\eta(\mathbf{f})}}{Z} \quad (9)$$

where

$$Z = \sum_{\mathbf{f} \in \Omega} e^{-U_\eta(\mathbf{f})}, \quad (10)$$

Z is a normalization constant, and $U_\eta(\mathbf{f})$ is an energy function defining the interaction between the MRF sites. The binary assumption for the label associated with the random field suggests the utilization of the Ising autologistic model [34], where a first order neighborhood that includes the nearest 6 voxels is considered. In the reconstruction case, the interaction between voxels in the neighborhood prevents the sudden growth of isolated or many irregular regions. The considered interactions are given by cliques including two sites where one of the sites is the central voxel of the neighborhood.

An energy function used to solved the reconstruction problem is determined by using Bayes theory:

$$P(\mathbf{f} | \mathbf{d}) = \frac{P(\mathbf{f})P(\mathbf{d} | \mathbf{f})}{P(\mathbf{d})} \quad (11)$$

where $P(\mathbf{f} | \mathbf{d})$ is the posterior probability, $P(\mathbf{f})$ is the prior probability expressed by (9), $P(\mathbf{d})$ is a normalization factor and $P(\mathbf{d} | \mathbf{f})$ represents the conditional probability of the observation process (the angiographic projections)

given the object in reconstruction. Noise in the input projections is approximated by a normal distribution [35] as in Bresler *et al.* [36]. The posterior probability thus becomes:

$$P(\mathbf{f} | \mathbf{d}) = \frac{e^{-U(\mathbf{f})}}{Z_t} \quad (12)$$

where Z_t is a normalization factor. By selecting the *maximum a posteriori* (MAP) estimator, the configuration of the 3-D object that maximizes the posterior probability is obtained. This leads to the minimization of the energy function $U(\mathbf{f})$ which is expressed as:

$$U(\mathbf{f}) = U_\eta(\mathbf{f}) + aU_{\mathbf{d}}(\mathbf{f}) \quad (13)$$

where a is a weighting parameter. The term $U_\eta(\mathbf{f})$ represents the internal energy of the 3-D random field of the object in reconstruction. This energy term models the prior constraints related to the smoothness of the object. It plays an important role in regularization since it reduces the effect of the ill-posed nature of the problem [37]. In our case, we use a neighborhood which consists of the 26 closest neighbors of each voxel. The energy term is chosen as:

$$U_\eta(\mathbf{f}) = \sum_{(i,j,k) \in \mathbf{L}} \left(\sum_{(q,r,s) \in \eta_{ijk}} [1 - \delta(f_{ijk} - f_{qrs})] \right) \quad (14)$$

where $\delta(\cdot)$ is the delta Kronecker function which takes on the value 1 if $f_{ijk} = f_{qrs}$ and zero otherwise. The term $U_{\mathbf{d}}(\mathbf{f})$ is represented by a quadratic error whose minimization leads to realizations of the 3-D object that provides synthesized projections close to the corresponding input projections. The synthesized projections are generated according to the procedure specified in Section II-B. This term is expressed as:

$$U_{\mathbf{d}}(\mathbf{f}) = \sum_{(l,m)} (h1_{lm} - d1_{lm})^2 + \sum_{(u,v)} (h2_{uv} - d2_{uv})^2 \quad (15)$$

where $h1_{lm}$ and $h2_{uv}$ are the gray-level of pixels in the synthesized projections of the object in reconstruction, and $d1_{lm}$ and $d2_{uv}$ are the grey-level of the pixels in the input projections.

2) *Metropolis Based Optimization procedure:* During the optimization procedure, the initial ellipsoidal 3-D object is progressively deformed by minimizing the energy function. This optimization procedure is guided by a stochastic relaxation algorithm, which requires a proper choice of the weighting parameter a associated with the energy function [18]. The deformation of the initial 3-D object is performed by the simulation of a Gibbs Random Field. The optimization procedure works by generating realizations of the random process according to the Gibbs distribution. These realizations minimize the energy function, and they are generated according to the following procedure: each iteration of the optimization process implies visitation of each voxel included in a "target" region around the contour of the object in reconstruction. The criterion that has been used for defining this region is the following: a voxel belongs to the "target" region if the number of voxels in a $3 \times 3 \times 3$ neighborhood having a value different from the central voxel is greater than 8. This value was obtained during the training procedure presented in Section III-D. The stochastic relaxation algorithm used during the optimization of the conditional probability includes a simulated annealing algorithm that avoids the possibility of the optimization procedure becoming trapped

in a useless local minima. This implies the introduction of a temperature parameter $T(\tau)$ in the joint probability distribution function of (12) that results in the following equation:

$$P(\mathbf{f} | \mathbf{d}) = \frac{e^{-\frac{U(\mathbf{f})}{T(\tau)}}}{Z_t}. \quad (16)$$

The temperature value is decreased at each iteration. The initial temperature value $T(0)$ is taken high enough, such that a large number of proposed voxel modifications are allowed at the beginning of the optimization process. The final solution corresponds to the MAP estimator and is attained by progressively decreasing the temperature value while the iteration number is increased. In this case, we adopted the temperature decreasing law proposed by Kirkpatrick *et al.* [38]. The criteria used to decide whether the voxel under consideration is changed is based on the comparison between the probability value associated with the present configuration and the probability value associated with the configuration that would result after acceptance of the proposed voxel modification. This comparison between both probability values is estimated according to (12) and can be performed by estimating the change in energy associated with each new configuration [18]. The new configuration is accepted according to the Metropolis decision rule for a given temperature value. Each time a voxel is modified, the synthesized projections are updated as a function of the voxel modification. The energy function in (13) includes a weighting parameter. The choice of this value and the initial temperature is performed empirically using a training data set. The stopping criterion for the iterative optimization procedure implies counting the number of accepted transitions for the voxel set associated with the contour region. If the number of transitions is lower than 10 % of the total number of voxels included in this region, then the optimization procedure is stopped. For selecting this threshold value, several tests were performed and the threshold value that gave the best results in terms of 2-D and 3-D errors with respect to the number of iterations required was retained. Other threshold values could be chosen (for instance, values as low as 5 % or 1 %), but the number of iteration increases considerably and the reconstruction error does not improves accordingly. Alternatively, the algorithm could be run for pre-specified number of iterations. The entire algorithm is summarized in Fig. 3.

E. Space-time extension of the Markov model

The 3-D reconstruction from an entire sequence of biplane angiograms can be improved by considering the assumption that the left ventricle shape varies only slightly between two consecutive time instants during the cardiac cycle. The first stage in the reconstruction process starts by performing the reconstruction for the time instant t_0 in the image sequence, according to the method previously presented. Reconstruction at the instant t works under the assumption that the 3-D reconstruction for the instant $t-1$ is available and that this reconstruction gives the initialization shape. The improvement stage obtains the final reconstruction. A space-time neighborhood (see Fig. 4) for modeling the smoothness in the shape variation along the cardiac cycle is obtained by including the voxel $f_{ijk,t-1}$ in the neighborhood considered at time t . In this neighborhood structure, several types of cliques can be considered. A temporal clique including the voxels $f_{ijk,t}$ and $f_{ijk,t-1}$ in the neighborhood considered at time t is incorporated in the internal energy term $U_\eta(\mathbf{f})$ of (14). This clique is weighted by a coefficient that is different

Require: a : weighting coefficient for the energy function

Require: $T(0)$: initial temperature parameter

Require: $MaxIter$: max number of iterations

- 1: Initialize using an ellipsoidal shape
- 2: **for** an iteration number lower than $MaxIter$ **do**
- 3: Obtain a region R_c around the contour
- 4: **while** non-visited voxels in R_c
- 5: Select a voxel at random and without replacement
- 6: Select the new possible label as the complement of
the current label
- 7: Evaluate ΔU for the new label
- 8: **if** $\Delta U < 0$ **then**
- 9: Update voxel value
- 10: Update projections
- 11: **else**
- 12: Evaluate $p = \exp(\frac{-\Delta U}{T})$
- 13: Obtain a random number r_a
- 14: **if** $r_a > p$ **then**
- 15: Update voxel value
- 16: Update projections
- 17: **end if**
- 18: **end if**
- 19: **end while**
- 20: decrement T
- 21: **end for**

Fig. 3. Algorithm for the MRF based reconstruction

from the coefficients affecting the spatial cliques. This weighting coefficient is denoted β_t and its value defines the smoothness degree for modeling the temporal similarity between two consecutive 3-D reconstructed shapes. The new energy function term modeling the smoothness constraint can be expressed as:

$$U_{\eta}(\mathbf{f}) = \sum_{(i,j,k) \in \mathbf{L}} \left(\sum_{(q,r,s) \in \eta_{ijk}} [1 - \delta(f_{ijk} - f_{qrs})] + \beta_t [1 - \delta(f_{ijk,t} - f_{ijk,t-1})] \right) \quad (17)$$

where η_{ijk} denotes the spatial neighborhood at time instant t .

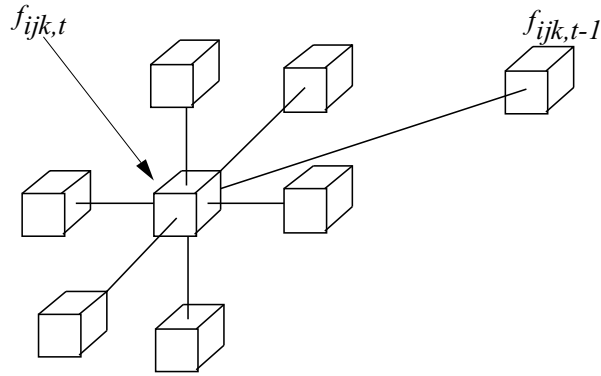
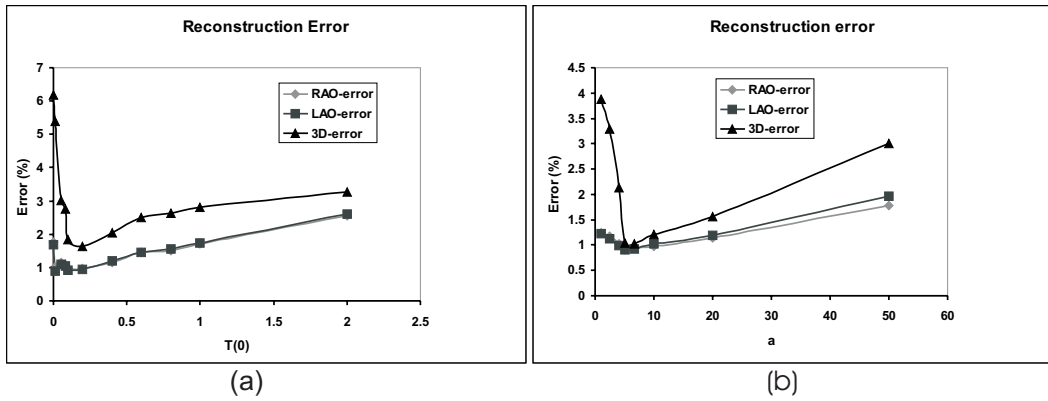


Fig. 4. Space - time neighborhood

Fig. 5. Choice of algorithm parameters. The reconstruction error (2-D and 3-D) is shown. a) as a function of parameter $T(0)$, b) as a function of parameter a .

III. RESULTS AND DISCUSSION

The reconstruction method was tested using mathematically synthesized phantoms and two binary databases. Additionally, the method was also tested using experimental data corresponding to a pair of sequences of real biplane ventriculograms. Visualization of the three-dimensional databases is performed using the Visualization ToolKit (VTK) [39].

A. Mathematically synthesized phantoms

Ellipsoidal objects are shapes useful for modeling the left ventricle [40]. This primitive is described according to the following equation:

$$\frac{(x - x_c)^2}{a^2} + \frac{(y - y_c)^2}{b^2} + \frac{(z - z_c)^2}{c^2} = 1 \quad (18)$$

where a, b and c are the semi-axes lengths of the ellipsoid centered at the point (x_c, y_c, z_c) . This basic shape can be deformed for generating shapes useful for testing the reconstruction algorithm. This can be done by introducing

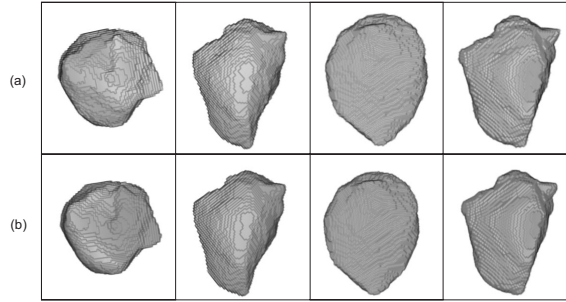


Fig. 6. Results for the reconstruction approach for the first binary database. a) 3-D binary database. b) Final 3-D binary reconstructed object. Both 3-D objects have a resolution of $80 \times 80 \times 80$ voxels.

weighting functions that scale the coordinates of the original shape denoted (x, y, z) to obtain the coordinates of the transformed object (X, Y, Z) as:

$$X = (\alpha z + 1)x; \quad Y = (\beta z + 1)y; \quad Z = z \quad (19)$$

where α and β are two parameters that define the degree of global deformation of the ellipsoidal shape (see Fig. 9).

B. 3-D databases and ventriculographic sequence images

A test of the reconstruction method was performed using two 3-D binary databases. The first is obtained by manual segmentation of a dog heart in a 3-D CT image. The interior of the heart is filled with 1 values and the exterior is filled with 0 values. The size of the database is $80 \times 80 \times 80$ voxels. The second 3-D binary database is the 3-D shape of the LV obtained from SPECT images of a human heart using a deformable model [41]. The size of this database is the same as the size of the first one. The projections of each binary database are synthesized by using the pin-hole projection model. This model simulates the conical projection geometry of an X-ray cineangiographic equipment. The parameters of the projection matrix correspond to the values obtained from the calibration of a biplane angiographic system. A pair of images is synthesized, each one with a size of 512×512 pixels and 8 bits per pixel.

The tests on real data of the reconstruction method are performed on two real ventriculographic image sequences of humans. These images were acquired with a Siemens X-ray biplane angiographic system, considering two standard examination views (Left Anterior Oblique-LAO 60° and Right Anterior Oblique-RAO 30°), with a field of view of 27 cm, a frame rate of 25 images per second and a total acquisition time of about one second including an entire cardiac cycle going from one end-systole to the next end-systole. The spatial resolution of the images is 512×512 pixels, with a depth of 8 bits. Other orientations of the biplane gantry with respect to the heart are feasible but the difference between both views should be close to 90° to provide complementary information about the LV shape. The images for the end-diastole instant in the first sequence of biplane angiograms are shown in Fig. 11. The acquisition chain includes the following steps:

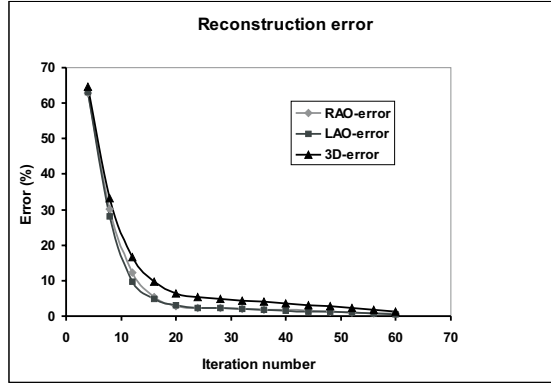


Fig. 7. Percent error in function of the iteration number, for the first binary database.

- 1) Distortion correction (of X-ray beam inhomogeneities, scattering effects, image intensifier-curvature and the magnetic field effects). This is done according to the procedure presented in Section II-A.
- 2) Calibration, which is performed according to the procedure reported in [25] from the acquired X-ray projections of the phantom, for both viewing angles of the bi-plane radiological system.
- 3) Acquisition of mask sequences of uncontrasted images.
- 4) Acquisition of contrasted sequences after dye medium injection in the left ventricle cavity.

C. Error measures

The error of the reconstructed object is measured by one of the following procedures, depending on the data available: a) When a 3-D reference binary object is available the 3-D reconstruction error is evaluated by comparing the 3-D reconstructed object to the reference object according to the following equation [42]:

$$3DError(\%) = \frac{\sum_{i=1}^{N_1} \sum_{j=1}^{N_2} \sum_{k=1}^{N_3} |f_{ijk} - \hat{f}_{ijk}|}{\sum_{i=1}^{N_1} \sum_{j=1}^{N_2} \sum_{k=1}^{N_3} f_{ijk}} \times 100 \quad (20)$$

where \hat{f}_{ijk} is a voxel in the reconstructed object and f_{ijk} is a voxel in the reference object.

- b) When the reference object is not available, the error is obtained by comparing the projection of the reconstructed

object to the input projection. The reconstruction error can be estimated through the following equation:

$$\begin{aligned}
 RAO - error(\%) &= \frac{\sum_{l=1}^{N_4} \sum_{m=1}^{N_5} |d1_{lm} - h1_{lm}|}{\sum_{l=1}^{N_4} \sum_{m=1}^{N_5} d1_{lm}} \times 100 \\
 LAO - error(\%) &= \frac{\sum_{u=1}^{N_4} \sum_{v=1}^{N_5} |d2_{uv} - h2_{uv}|}{\sum_{u=1}^{N_4} \sum_{v=1}^{N_5} d2_{uv}} \times 100
 \end{aligned} \tag{21}$$

where the pixel intensity values of the input projections are denoted as $d1_{lm}$ and $d2_{uv}$ and the pixel intensity values of the projections of the 3-D reconstructed object are denoted by $h1_{lm}$ and $h2_{uv}$.

D. Choice of the algorithm parameters

The parameters defining the performance of the 3-D reconstruction for a given time instant are a , $T(0)$ and the number of iterations. These parameters have been chosen empirically, after performing several tests, as the set that gives the least 3-D and 2-D reconstruction error. The reconstruction method is first trained by considering the two binary databases (training set). The procedure consists in changing the value of one of the parameters while keeping the other parameters constant. The 2-D and 3-D reconstruction errors are measured and the selected value for this parameter, that gives the lower reconstruction errors, is kept constant when the other parameter is studied at the next iteration. This procedure is repeated until the optimal parameter set is obtained. This parameter set is further tested with the biplane ventriculographic image sequence. The optimal values are $a = 5$ and $T(0) = 0.1$. In Fig. 5a the variation of the reconstruction error, evaluated according to (20) and (21), is shown as a function of the parameter $T(0)$ considering a maximum number of 64 iterations and a value of the parameter a equal to 5. The minimum 3-D error is obtained with the value of $T(0) = 0.1$. In Fig. 5b the variation of the reconstruction error (2-D and 3-D) is shown as a function of a , considering a maximum number of 64 iterations and $T(0) = 0.1$. The optimal value for a is 5. In Fig. 7, the variation of the reconstruction error is shown as a function of the number of iterations. The optimal values for parameters a and $T(0)$ are chosen ($a = 5$, $T(0) = 0.1$). The results show that both the 3-D error and 2-D error attain smoothly the minimum value in about 60 iterations. From these results it is possible to verify that when we use a set of parameters giving the minimum 3-D error, the 2-D error is also minimum. Regarding the sensitivity of the reconstruction method to each one of the parameters, it is possible to appreciate that there is a relative wide range of parameter values that could be used without severely affecting the performance of the reconstruction algorithm. For instance, a variation of the parameter a from 5 to 50 has as a consequence an increase of the 3-D reconstruction error from 1.7% to 5%. In general using parameters values such that $a < 1$ and $T(0) < 0.05$ increases the 3-D percent error, however the algorithm is less sensible when using higher values for these parameters. Additionally the threshold defining the target region in Section II-D.2 has been selected by varying the value between 3 and 24 and retaining the value that gave the lower 3-D error

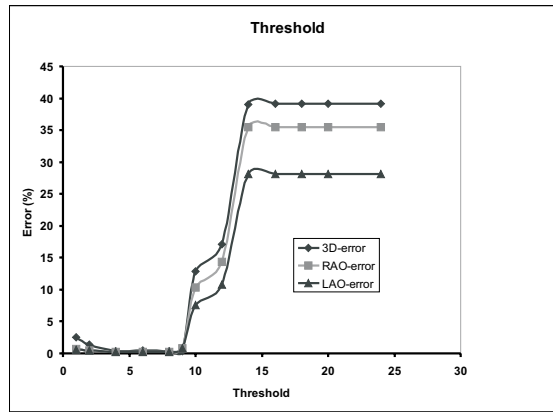


Fig. 8. Percent reconstruction error versus threshold used for defining the target region

using 64 iterations. The optimal value found was 8. If this threshold value is increased the number of voxels in the target region is decreased and the number of iterations required for attaining a low 3-D error is increased. When the threshold value is decreased the number of voxels in the target region is increased, the reconstruction error is reduced slightly but the execution time is increased substantially. The percent error versus the threshold value is shown in Fig. 8. The parameter β_t in (17) is selected as the value that provides the lower projection error when the algorithm is initialized with the 3-D reconstruction of the angiograms at time $t - 1$. An optimal value is obtained as $\beta_t = 2.0$.

E. Results using mathematically synthesized phantoms

A total of 124 phantoms with size $80 \times 80 \times 80$ were generated by changing parameters $\{a, b, c, \alpha, \beta\}$ in (18) and (19). Parameters $\{a, b, c\}$ were varied in the $[20, 40]$ interval and parameters $\{\alpha, \beta\}$ were varied in the $[0.001, 0.05]$ interval. The parameters were varied to generate several sets of phantoms. In each set, one of the parameters is varied while the others are kept constant. Table I shows the parameter values used to generate the phantoms. Four of the mathematically synthesized phantoms are shown in Fig. 9, where the objects are rendered using the VTK according to a pair of views: the RAO view, shown in Fig. 9a, and the LAO view, shown in Fig. 9b. Two projections of each 3-D object were synthesized using the same projection matrices used for the 3-D binary databases. The reconstruction is performed from these projections using the optimal parameters. The 3-D and 2-D percent errors are measured after 64 iterations. Table II summarizes the 3-D percent error and Table III summarizes the 2-D error. Observe that even when the 3-D average error is $3.87 \pm 3.93\%$, the maximum percent error can be as high as 15.12%. This maximum error is obtained when the ambiguity of the 3-D object is high and the reconstruction algorithm is not able to recover the right orientation. In all cases, however, the average 2-D percent error for the RAO view (Table III) is $1.32 \pm 1.19\%$ and the average 2-D percent error for the LAO view is $1.13 \pm 0.82\%$. The maximum percent error for the RAO view is 6.79%, and 3.88% for the LAO view.

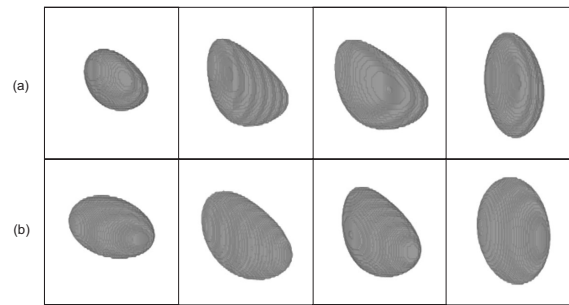


Fig. 9. Four 3-D mathematically synthesized phantoms included in the set of 124 used for testing the reconstruction algorithm. a) RAO view. b) LAO view. Each 3-D object has a resolution of $80 \times 80 \times 80$ voxels.

TABLE I
VARIATION OF PARAMETERS FOR PHANTOMS GENERATION.

Axes(a,b,c)	Step	α	Step	β	Step	Number of phantoms
40,20,30		0.0213		0.001-0.05	0.0163	30
40,20,30		0.025-0.049	5.85×10^{-4}	2×10^{-3}		41
40,21-31,30	1	0.0213		2×10^{-3}		11
20-39,20,30	1	8×10^{-3}		0.02		20
40,31-40,30	1	0.0213		0.02		10
25,40,26-33	1	8×10^{-3}		0.02		8
30,40,36-39	1	8×10^{-3}		0.02		4

F. Results using 3-D binary databases

Reconstruction results for the first binary database (see Fig. 6) show the 3-D object visualized from several view points. The final 3-D error is 1.37% after 64 iterations. The evolution of the 2-D and 3-D percent errors as a function of the iteration number is shown in Fig. 7. For the second binary database, we show (see Fig. 10) the original as well as the reconstructed objects visualized from several viewpoints. The final 3-D error is 2.7% after 80 iterations. An additional test using the first binary database was performed but in this case a resolution of $64 \times 64 \times 64$ voxels was considered. The evolution of the 2-D and 3-D percent errors as a function of the iteration number is similar to the one shown in Fig. 7 for the case of a resolution of $80 \times 80 \times 80$ voxels, however, the execution time is reduced because the number of voxels is lower.

TABLE II
3-D PERCENT ERROR FOR THE TESTS PERFORMED.

	Ellipsoids (Mean \pm Std deviation)	1st database	2nd database
3-D percent error	3.87 ± 3.93	1.37	2.70
Maximum error	15.12	–	–

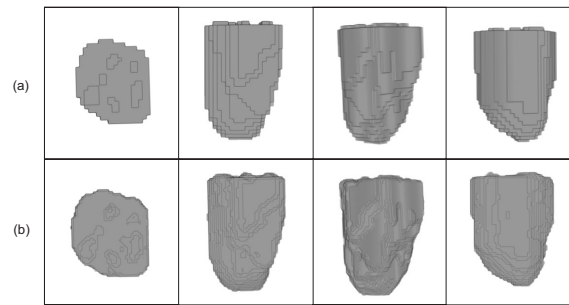


Fig. 10. Results for the reconstruction approach for the second binary database. a) 3-D binary database. b) Final 3-D binary reconstructed object. Both 3-D objects have a resolution of $80 \times 80 \times 80$ voxels.

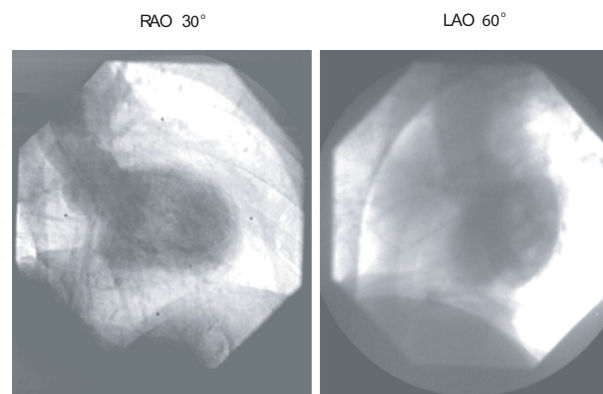


Fig. 11. Input angiograms extracted from the first sequence for the end-diastole. The size of the images is 512×512 pixels.

G. Tests on real data

The fact that the real 3-D object is not available makes it impossible to measure the 3-D reconstruction error directly. In this case the error assessment is performed by comparing the synthesized projection of the reconstructed object against the input projections (see Section III-C). Four time instants of the ventriculogram sequence are selected in order to adjust the algorithm parameters. These tests show that parameters obtained using the binary databases also provide the minimal projection error when performing the reconstruction from real ventriculograms.

1) *Test at the end-diastole instant:* 3-D reconstruction for the end-diastole instant of time, in the first sequence of angiograms, required 48 iterations to reach a projection error value of 6.67% and 7.92% for the LAO and RAO views respectively (see Fig. 13). We verified that more iterations do not improve nor degrade the projection error. The stopping criterion consists in measuring the projection error. At each iteration, if the projection error improvement is lower than 0.5% for both projections during three consecutive iterations or the pre-specified maximum number of iterations is attained, the algorithm is stopped. The reconstructed shape is spatially coherent and could match the real anatomic structure shape of the left ventricle. A careful examination of Fig. 11 (RAO incidence) shows that the assumption of perfect mixture of blood and contrast agent is not verified on these images. A visual examination

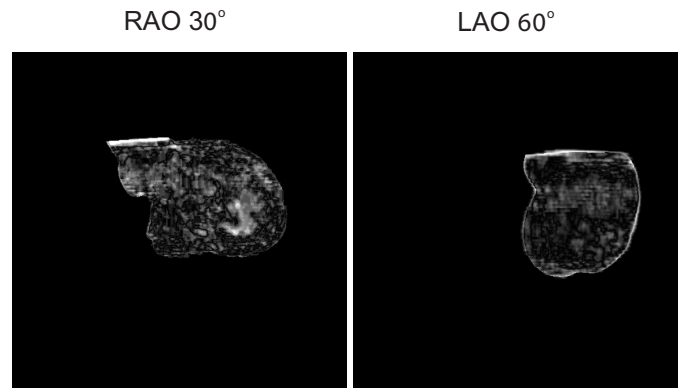


Fig. 12. Absolute value of the difference between the input images and the synthesized projections of the reconstructed object. A gray-level enhancement is performed in both images for visualizing the small differences. The size of the images is 512×512 pixels.

of the RAO image shows two dark regions located at the base and at the apex of the LV while there is a less dark region located in the middle portion of the LV. An alternative procedure for detecting the imperfect mixture of blood and dye agent consists in playing the sequence of cineangiograms and observing how the bubbles of un-mixed contrast agent evolve in time. This imperfect mixture of blood and contrast agent could affect the shape of the final reconstructed object as shown by the bulge that is visible in Fig. 13 for the "Right Apical" incidence. An additional test consists in performing the reconstruction of the LV chamber at the end-diastole instant in the second sequence of biplane angiograms. The input biplane angiograms are shown in Fig. 15. The reconstruction is performed using the same parameters (a , $T(0)$ and number of iterations) considered in the first sequence of angiograms. The reconstructed shape is shown in Fig. 16. In this case the projection error is 8.78% and 8.59% for the LAO and RAO views respectively.

2) *Test at the end-systole instant:* The same test has been performed to obtain the 3-D reconstruction of the left ventricle for the instant of end-systole by considering as the input projections the preprocessed images in the first sequence of angiograms. The same parameters as those considered for the previous test has been used. Results are shown in Fig. 14 where the reconstructed object is shown from several views. The minimum projection error value in this case is 11.7% for the LAO image and 13.5% for the RAO image after 48 iterations. This error value remains unchanged when the iteration count is increased.

3) *Test for the entire angiographic sequences:* The reconstruction is performed for two angiographic sequences, each comprising one cardiac cycle. The first sequence has 28 and the second sequence has 27 biplane images. Both steps of the reconstruction algorithm are considered at each time instant. Table III summarizes the 2-D percent error obtained. In this case, the average percent error for the RAO view of the first sequence is $9.51 \pm 1.38\%$ and $11.78 \pm 2.28\%$ for the LAO view. The maximum percent error for the RAO view is 12.01% and 15.00% for the LAO view. The average percent error for the RAO view of the second sequence is $9.50 \pm 1.82\%$ and $10.72 \pm 2.27\%$ for the LAO view. The maximum percent error for the RAO view is 12.81% and 15.35% for the LAO view. These errors could be explained by considering several sources including: the segmentation procedure (which does not take into

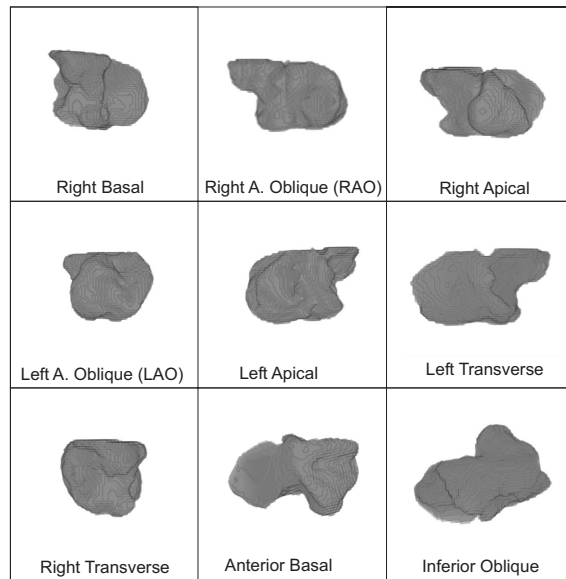


Fig. 13. 3-D reconstruction of the left ventricle for the end-diastole. The reconstruction is performed from angiograms extracted from the first sequence. The reconstruction is visualized from several points of view. The 3-D object has a resolution of $80 \times 80 \times 80$ voxels.

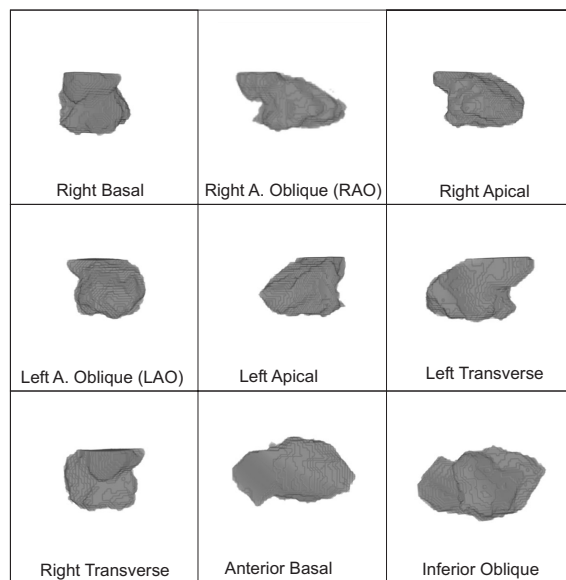


Fig. 14. 3-D reconstruction of the left ventricle for the end-systole. The reconstruction is performed from angiograms extracted from the first sequence. The reconstruction is visualized from several points of view. The 3-D object has a resolution of $80 \times 80 \times 80$ voxels.

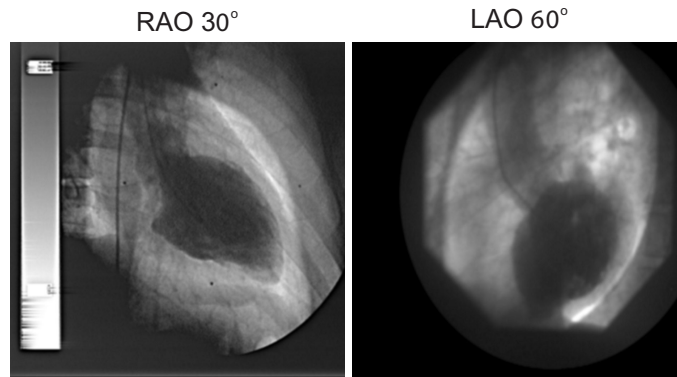


Fig. 15. Input angiograms extracted from the second sequence for the end-diastole. The size of the images is 512×512 pixels.

account the correspondence between both views), the imperfect mixture of blood and contrast agent, the quantum noise, the imperfection related to the subtraction mask and the brightness differences between both views. Their contribution could make both projections inconsistent for performing the 3-D reconstruction. As a consequence, the projection error increases considerably with respect to the projection error obtained using simulated data. From these sources of error the contribution of the inaccuracies related to segmentation are important. This can be verified in Fig. 12 where the absolute value of the difference between the original projection images for the end-diastole instant and the synthesized projections of the reconstructed object are shown. A contrast enhancement is applied to both images for visualizing the error. The pixels where the error is greater are shown with higher gray-level intensities and they are located mainly in the borders of the images. This is apparent in the LAO view where the projection error is greater. Additionally, as the 2-D projection error (in (21)) is proportional to the average considering all pixels in the shape, if the projection error for pixels near the contour is high and the size of the shape decreases (as is the case when the LV evolves from diastole to systole) then the projection error for the shape increases. This variation in the 2-D error is obtained when the entire angiographic sequence is reconstructed.

TABLE III
2-D PERCENT ERROR FOR THE TESTS PERFORMED.

	Ellipsoids (Mean \pm Std deviation)	1st database	2nd database	Angiography 1st sequence	Angiography 2nd sequence
2-D RAO percent error	1.32 ± 1.19	0.22	1.00	9.51 ± 1.38	9.50 ± 1.82
Maximum RAO percent error	6.79	–	–	12.01	12.81
2-D LAO percent error	1.13 ± 0.82	0.24	1.10	11.78 ± 2.28	10.72 ± 2.27
Maximum LAO percent error	3.88	–	–	15.00	15.35

4) *Test for the space-time Markov model:* The left ventricle 3-D reconstruction is also performed for the first biplane image sequence taking into account the space-time regularization term of (17). The 3-D reconstruction is

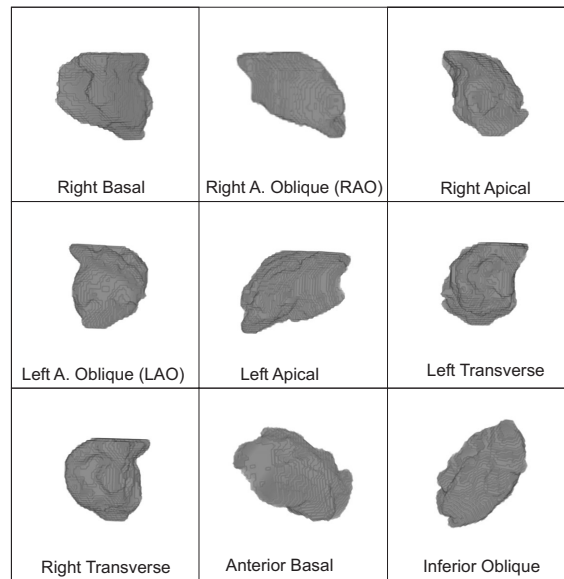


Fig. 16. 3-D reconstruction of the left ventricle for the end-diastole. The reconstruction is performed from angiograms extracted from the second sequence. The reconstruction is visualized from several points of view. The 3-D object has a resolution of $80 \times 80 \times 80$ voxels.

performed for this sequence for the images between time instants 0 and 27. The 3-D reconstruction for the time instant $t = 0$ includes two stages: approximate reconstruction and iterative refinement. Then, for images 1 to 27 the 3-D reconstructed object at the time instant t is used as initialization for performing the 3-D reconstruction at the time $t + 1$. The refinement process, which is based on the Markov Random Field, considers the same set of parameters (a and $T(0)$) as for the previous tests. The coefficient β_t is set to 2.0. The number of iterations required to have projection errors varying less than 0.5% in two consecutive iterations is 16. The reconstructed shapes are shown in Fig. 17. Visualization of the 3-D ventricle for each instant of the cardiac cycle according to the RAO 30° view allows one to appreciate that the reconstructed object gradually changes and its shape remains close to the left ventricle shape observed in the 2-D angiograms. The temporal constraint is aimed at preventing abrupt variations in shape between the objects reconstructed at two consecutive time instants. In this paper, our results are of qualitative nature: they show that the reconstructed objects agree with what is expected, that is, a smooth transition in shape over time.

H. Comparison with respect to other reconstruction methods

The method proposed by Prause and Onnash [9] is validated using the real biplane images of a dye-filled bottle obtaining 3-D shape errors of about 18.0%, whereas for error-free projection data the 3-D error is 3.4%. The method is also tested using biplane images of a LV shaped phantom. The 3-D error for the reconstruction from real biplane images is 12.7% while for error-free projections is 2.0%. Our results using synthesized phantoms could be compared with the results reported in [9] for error-free projections obtaining 3-D error values close to their results (see Table II). Their results using real biplane images provide 3-D errors between 12.7% and 18%. In our case,

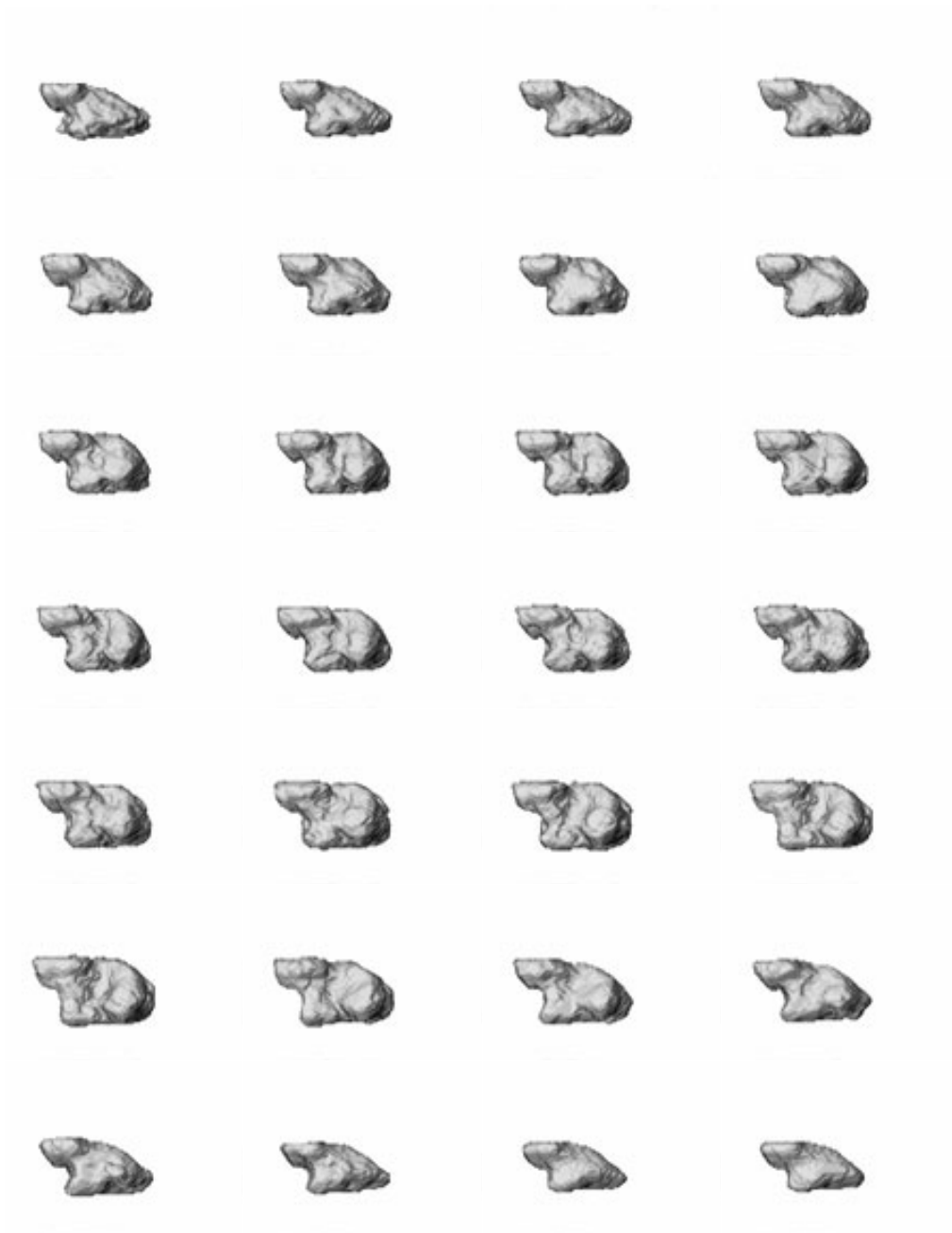


Fig. 17. Visualization of left ventricle 3-D reconstruction for a cardiac cycle of the first sequence of angiograms. The reconstruction is performed using the space-time regularization term of (17). Each reconstructed object is visualized according to the RAO 30° view.

when the reconstruction is performed from real angiograms, the 2D projection errors are between 9.5 % and 11.7 %. These errors are given in different spaces (3-D and 2-D) and a direct comparison is therefore not possible. The method in [9] is also tested using several *in vivo* biplane angiograms, however, the projection error is not provided. The method proposed by Kehl *et al.* [12] performed the comparison in terms of the volume measurement of the reconstructed object with respect to the true volume of the phantom or post-mortem hearts. A regression line was obtained in each case showing a good correlation ($V_{true} = 1.049V_{measured} - 0.75[ml]$). Unfortunately no other quantitative measurement was performed for validating the accuracy of the reconstructed shape. The reconstruction method proposed in [16] is tested using the same binary databases and the first sequence of angiograms used for validating the method reported in this paper. In that case, the 3-D error for the binary databases is 6.48 % and 8.0 % respectively. The 2-D error for the end-diastole instant is 7.9 % for the LAO view and 7.2 % for the RAO view. However the average errors for the entire sequence are 11.30 % for the LAO view and 12.0 % for the RAO view. This shows that the Markov Random based reconstruction method performs better than the fuzzy and evidential based method. The method proposed by Moriyama *et al.* [10] only takes into account the contour information of the angiograms and the reconstruction error is given in terms of the average distance between points of the LV contour in the input angiograms with respect to the contour points of the projected reconstructed shape. When only two views are considered for performing the reconstruction the average error is 4.9 mm. In this case, a comparison in terms of 3-D error is not possible. The slice based method proposed by Slump and Gerbrands [7] quantifies the reconstruction error using an equation similar to (21). The reconstruction error for noise-free projections is 8.0 %. In general, only a few methods can be compared directly with respect to our method in terms of 3-D errors. In these cases, our method shows a similar or slightly better performance. We note, however, that an adequate comparison is only possible by testing the different algorithms using the same input data.

IV. CONCLUSIONS

Our contributions towards the solution of the reconstruction of the left ventricle from two angiographic views are:

- 1) Consideration of a space-time Markov Random Field Model and simulated annealing to guide a model-based reconstruction algorithm.
- 2) Consideration of the real conical geometry in the reconstruction process that gives a more realistic approach, simplifies the preprocessing stages and enables the reconstruction directly in 3-D space.

The results obtained with mathematical synthesized objects, two binary databases as well as with real angiographic data are promising. When the reconstruction is performed from two angiographic views, the inclusion of the acquisition geometry simplifies the pre-processing stages, as the magnification and intensity distortion are implicitly considered in the reconstruction process. The reconstruction method is flexible because it is possible to modify the energy function in order to include additional constraints. So for example, a temporal constraint has been included to optimize the reconstruction through the image sequence. Another advantage of our reconstruction method is related to the fact that the reconstruction process is performed directly in the 3-D space, so it is also possible to reduce

the uncertainty of orientation choice in the 2-D slice plane, which is an important limitation of the slice-based reconstruction methods. One important drawback of the method is the hypothesis of contrast medium homogeneity, which is not easy to attain except if the injection is initiated at the rapid filling phase of diastole; one way to achieve this is by ECG-triggered control [43]. If the mixture of blood and contrast agent in the LV is inhomogeneous, the reconstructed shape will be distorted, and may include holes where there are un-mixed blood bubbles and bulges where there are bubbles of un-mixed contrast agent. The other limitation of the reconstruction method is the fact that uniqueness of the solution cannot be guaranteed. This is a common limitation for reconstruction algorithms that operate from only two views. In our view, the flexibility of the algorithm in terms of the energy function coding capabilities compensates for this limitation. The 3-D object orientation and the approximate primitive shape of the LV are further information that can be included in the formulation. The clinical objective for the reconstruction process is related to the execution time of the algorithm. For diagnostic purposes, it is possible to perform the reconstruction procedure and analysis off-line. The execution time constraints are more stringent when performing interventional work, as the results are required almost on-line. Concerning the execution time, our left ventricle reconstruction algorithm fits within the diagnostic objectives as the reconstruction program takes about 3 minutes for reconstructing each 3-D image when running on a Silicon Graphics ORIGIN 2000. The program was also run on a personal computer with a Pentium IV processor at 1.90 GHz and 256 MB RAM for reconstructing the second sequence of angiograms. The average execution time was 258.25 ± 7.07 seconds when both stages of the algorithm are considered. This execution time could be lowered by optimizing the code and by implementing a parallel program version that could fit several computer architectures. Although the Metropolis based optimization algorithm using simulated annealing can prevent the optimization procedure from being trapped in local optimal values, it can be very slow if the volume size is increased for better resolution and representation. Other optimization procedures were tested including the Gibbs Sampler [18], the microcanonical Monte Carlo simulation [44] and the Iterative Conditional Modes (ICM) [45]. In general the Metropolis, the Gibbs sampler and the microcanonical Monte Carlo simulator have a similar performance in terms of final 3-D error and number of iterations required when tested on the binary databases. The ICM requires about 25 % of the iterations required for the stochastic methods to attain a 3-D error of 10 % but with this method no further improvements with respect to the reconstruction error are obtained. This result suggests using a multi-resolution algorithm starting at lower resolutions using stochastic optimization algorithms and then at higher resolution to switch to deterministic optimization algorithms like the ICM. In this way, an improvement in speed could be obtained.

ACKNOWLEDGMENT

This research was supported by CDCHT (grant: I-672-00-02-B) and CECALCULA of The Universidad de Los Andes in Venezuela as well as the BID-CONICIT and the French PCP Program.

REFERENCES

- [1] G. T. Herman, "Image reconstruction from projections," *Real-Time Imaging*, vol. 1, pp. 3–18, 1995.

- [2] S. Chang, "The reconstruction of binary patterns from their projections," *Communications of the ACM*, vol. 14, no. 1, pp. 21–25, 1971.
- [3] S. Chang and Y. Wang, "Three-dimensional object reconstruction from orthogonal projections," *Pattern Recognition*, vol. 7, pp. 167–176, 1975.
- [4] S. K. Chang and C. K. Chow, "The reconstruction of three-dimensional objects from two orthogonal projections and its application to cardiac cineangiography," *IEEE Transactions on Computers*, vol. C-22, pp. 18–28, Jan. 1973.
- [5] D. G. Onnasch and P. H. Heintzen, "A new approach for the reconstruction of the right or left ventricular form from biplane angiography recordings," in *Proceedings of Computers in Cardiology*, IEEE Computer Society, USA, 1976, pp. 67–73.
- [6] D. G. Onnasch, "A concept for the approximate reconstruction of the form of the right or left ventricle from biplane angiograms," in *Roentgen-Video Techniques for dynamic studies of structure and function of the Heart and Circulation*, P. H. Heintzel, Ed. Stuttgart: Thieme-Verlag, 1978, pp. 235–242.
- [7] H. Cornelis and J. J. Gerbrands, "A network flow approach to reconstruction of the left ventricle from two projections," *Computer Graphics and Image Processing*, vol. 18, pp. 18–36, 1982.
- [8] Y. Wang, P. A. Heng, and F. M. Wahl, "Image reconstructions from two orthogonal projections," *International Journal of Imaging Systems and Technology*, vol. 13, pp. 141–145, 2003.
- [9] G. Prause and D. G. Onnasch, "Binary reconstruction of the heart chambers from biplane angiographic image sequences," *IEEE Transactions on Medical Imaging*, vol. 15, no. 4, pp. 532–546, 1996.
- [10] M. Moriyama, Y. Sato, H. Naito, M. Hanayama, T. Ueguchi, T. Harada, F. Yoshimoto, and S. Tamura, "Reconstruction of time-varying 3-D left-ventricular shape from multiview X-ray cineangiocardiograms," *IEEE Transactions on Medical Imaging*, vol. 21, no. 7, pp. 773–785, 2002.
- [11] Y. Sato, M. Moriyama, M. Hanayama, H. Naito, and S. Tamura, "Acquiring 3-D models of nonrigid moving objects from time and viewpoint varying image sequences: A step toward left ventricle recovery," *IEEE Transactions on Pattern Analysis and Machine Intelligence*, pp. 253–258, 1997.
- [12] H. Kehl, J. Jäger, N. Papazis, D. Dimitrelos, J. Gehrman, R. Kassenböhmer, J. Vogt, and G. Sakas, "3D heart modelling from biplane, rotational angiocardiographic X-ray sequences," *Computer & Graphics*, pp. 731–739, 2000.
- [13] R. Medina, "Reconstruction tridimensionnelle du ventricule gauche en angiographie bi-plan," Ph.D. dissertation, University of Rennes 1, Rennes, France, 1998.
- [14] R. Medina, M. Garreau, H. Lebreton, and D. Jugo, "Three-dimensional reconstruction of the left ventricle from two angiographic views," in *Proceedings of The Nineteenth Annual International Conference of the IEEE Engineering in Medicine and Biology Society*, Chicago, IL, 1997, pp. 569–572.
- [15] J. Toro, R. Medina, M. Garreau, D. Jugo, and H. Carrasco, "Left ventricle 3D reconstruction using gibbs random fields and simulated annealing," in *Proceedings of the I International Seminar of Simulation and Modelling in Bioengineering*, Computational Mechanics Publications, Southampton, UK, 1996, pp. 239–248.
- [16] R. Medina, M. Garreau, J. Toro, J. L. Coatrieux, and D. Jugo, "Three-dimensional reconstruction of the left ventricle from two angiographic views: An evidence combination approach," *IEEE Transactions on Systems, Man, and Cybernetics-Part A: Systems and Humans*, vol. 34, no. 3, pp. 359–370, 2004.
- [17] R. Medina, M. Garreau, C. Navarro, J. Coatrieux, and D. Jugo, "Reconstruction of the left ventricle shape from two angiographic views: a fuzzy and evolutionary approach," in *Proceedings of the IEEE Computers in Cardiology*, Hannover, Germany, 1999, pp. 663–666.
- [18] S. Geman and D. Geman, "Stochastic relaxation, gibbs distribution, and the bayesian restoration of images," *IEEE Transactions on Pattern Analysis and Machine Intelligence*, vol. 6, no. 6, pp. 721–741, 1984.
- [19] J. Besag, "Spatial interaction and the statistical analysis of lattice systems," *Journal of the Royal Statistical Society*, vol. 36, no. 2, pp. 192–236, 1974.
- [20] J. Marroquin, "Optimal bayesian estimators for image segmentation and surface reconstruction," Massachusetts Institute of technology, Artificial Intelligence Laboratory, Tech. Rep. Memo 839, 1985.
- [21] S. Z. Li, *Modeling Image Analysis Problems Using Markov Random Fields*, R. Chellappa and A. Jain, Eds. Boston, MA: Academic Press, 1993.
- [22] H. Derin and H. Elliot, "Modeling and segmentation of noisy and textured images using gibbs random fields," *IEEE Transactions on Pattern Analysis and Machine Intelligence*, vol. 9, no. 1, pp. 39–55, 1987.

- [23] C. Pellot, A. Herment, M. Sigelle, P. Horain, H. Maître, and P. Peronneau, "A 3D reconstruction of vascular structures from two X-ray angiograms using an adapted simulated annealing algorithm," *IEEE Transactions on Medical Imaging*, vol. 13, no. 1, pp. 48–60, Mar. 1994.
- [24] T. Tian and M. Shah, "Motion estimation and segmentation," *Machine Vision and Applications*, vol. 9, pp. 32–42, 1995.
- [25] P. Haigron, "Numérisation de surfaces tridimensionnelles application à la fabrication de prothèses personnalisées," Ph.D. dissertation, The University of Rennes I, Image and Signal Processing Laboratory (LTSI), France, 1993.
- [26] M. Levoy, "Efficient ray tracing of volume data," *ACM Transactions on Graphics*, vol. 9, no. 3, pp. 245–261, 1990.
- [27] R. R. Galigekere, K. Wiesent, and D. W. Holdsworth, "Cone-beam reprojection using projection-matrices," *IEEE Transactions on Medical Imaging*, vol. 22, no. 10, pp. 1202–1214, 2003.
- [28] R. Haralick and L. Shapiro, *Computer and Robot Vision*. New York: Addison-Wesley Publishing Company, 1993.
- [29] S. Jaggi, W. C. Karl, and A. S. Willsky, "Estimation of dynamically evolving ellipsoids with applications to medical imaging," *IEEE Transactions on Medical Imaging*, vol. 14, pp. 249–258, 1995.
- [30] P. Milanfar, W. C. Karl, and A. S. Willsky, "Reconstructing binary polygonal objects from projections: A statistical view," *CVGIP: Graphical Models and Image Processing*, vol. 56, no. 5, pp. 371–391, 1994.
- [31] R. N. Ghanem, C. Ramanathan, P. Jia, and Y. Rudy, "Heart-surface reconstruction and ecg electrodes localization using fluoroscopy, epipolar geometry and stereovision: Application to noninvasive imaging of cardiac electrical activity," *IEEE Transactions on Medical Imaging*, vol. 22, no. 10, pp. 1307–1318, 2003.
- [32] W. Karl, G. Verghese, and A. Willsky, "Reconstructing ellipsoids from projections," *Graphical Models and Image Processing*, vol. 56, no. 2, pp. 124–139, 1994.
- [33] T. F. Cootes and C. J. Taylor, "Statistical models of appearance for computer vision," University of Manchester, Wolfson Image Analysis Unit, Tech. Rep., 2001.
- [34] J. Besag, "Nearest-neighbour systems and the auto-logistic model for binary data," *Journal of the Royal Statistical Society*, vol. 34, pp. 75–83, 1972.
- [35] E. Dougherty, *Probability and Statistics for the Engineering, Computing and Physical Sciences*. Englewood Cliffs, U.S.A: Prentice-Hall, 1990.
- [36] Y. Bresler and A. Macovski, "Three-dimensional reconstruction from projections with incomplete and noisy data by object estimation," *IEEE Transactions on Acoustics, Speech, and Signal Processing*, vol. 35, no. 8, pp. 1139–1152, 1987.
- [37] M. Bertero, T. Poggio, and V. Torre, "Ill-posed problems in early vision," Massachusetts Institute of Technology, Artificial Intelligence Laboratory, Tech. Rep. AI-memo no. 924, 1987.
- [38] S. Kirkpatrick, C. Gelatt, and M. Vecchi, "Optimization by simulated annealing," in *Readings in Computer Vision*, M. Fischler and O. Firschein, Eds. U.S.A.: IBM Thomas J. Watson Research Center, 1982, pp. 606–615.
- [39] W. Schroeder, K. Martin, and B. Lorensen, *The Visualization Toolkit*. Upper Saddle River, NJ: Prentice-Hall, 1998.
- [40] W. Chang, T. Huang, and M. Arrow, "Modeling, analysis and visualization of left ventricle shape and motion by hierarchical decomposition," *IEEE Transactions on Pattern Analysis and Machine Intelligence*, vol. 16, no. 4, pp. 342–356, 1994.
- [41] X. Riot, "Quelques aspects de l'imagerie 3D et de telemedecine," Ph.D. dissertation, The University of Rennes 1, Image and Signal Processing Laboratory (LTSI), France, 1997.
- [42] C. Slump and J. Gerbrands, "A network flow approach to the reconstruction of the left ventricle from two projections," *Computer Graphics And Image Processing*, vol. 18, no. 1, pp. 18–36, 1982.
- [43] H. Lehmkuhl, T. Machning, B. Eicker, K. Barth, K. Reynen, and K. Bachmann, "Digital subtraction angiography: Feasibility of densitometric measurements obtained by monoplane area-length-method," in *Proceeding of the IEEE Computers in Cardiology*, London, 1993, pp. 29–32.
- [44] M. Creutz, "Microcanonical monte carlo simulation," *Physical Review Letters*, vol. 50, no. 19, pp. 1411–1414, 1983.
- [45] J. Besag, "On the statistical analysis of dirty pictures," *Journal of the Royal Statistical Society, part B*, vol. 48, pp. 259–302, 1986.